DEVELOPMENT OF AN LES METHODOLOGY FOR COMPLEX GEOMETRIES

ELIA MERZARI* and HISASHI NINOKATA
Research Laboratory for Nuclear Reactors, Tokyo Institute of Technology
N1-5 2-12-1, O-Okayama Meguro-ku, Tokyo
*Corresponding author. E-mail : merzari@nr.titech.ac.jp

Invited March 25, 2008
Received October 30, 2008

The present work presents the development of a Large Eddy Simulation (LES) methodology viable for complex geometries and suitable for the simulation of rod-bundles. The use of LES and Direct Numerical Simulation (DNS) allows for a deeper analysis of the flow field and the use of stochastical tools in order to obtain additional insight into rod-bundle hydrodynamics.

Moreover, traditional steady-state CFD simulations fail to accurately predict distributions of velocity and temperature in rod-bundles when the pitch (P) to diameter (D) ratio P/D is smaller than 1.1 for triangular lattices of cylindrical pins. This deficiency is considered to be due to the failure to predict large-scale coherent structures in the region of the gap.

The main features of the code include multi-block capability and the use of the fractional step algorithm. As a Sub-Grid-Scale (SGS) model, a Dynamic Smagorinsky model has been used. The code has been tested on plane channel flow and the flow in annular ducts. The results are in excellent agreement with experiments and previous calculations.

KEYWORDS : LES, CFD, Complex Geometries

1. INTRODUCTION

Traditional steady-state CFD does not always yield sufficiently accurate distributions of velocity, temperature, and shear stress for tight fuel bundles. An unsteady simulation is often necessary to correctly reproduce the flow field [1], which is characterized by large-scale coherent structures [2].

Two main approaches are usually employed to study unsteady flows: the direct numerical solution of the Navier-Stokes equations (DNS) and Large Eddy Simulation (LES). LES has gained popularity in recent years [3] because of the availability of increasing computing power, and because of its lower computational cost compared with DNS. In LES only the larger scales of motion are resolved (corresponding to the higher part of the Kolgomorov spectra), while the smaller scales have to be modelled

Another possible solution is the adoption of an Unsteady Reynolds Averaged Navier Stokes (URANS) simulation [4]. The implementation of such an approach permits the use of much coarser grids (in comparison to DNS and LES) and holds the promise of providing a general methodology for the prediction of the flow field of rod bundles with arbitrary geometric parameters [1] at a reasonable computational cost.

LES and DNS are of academic interest in themselves, since they allow for a deeper analysis of the flow field and the use of stochastical tools [5] like Proper Orthogonal Decomposition (POD). In the present work the development of a flexible LES methodology for complex flows (and its implementation into a code) will be considered. Its main features are:

- Solution of the Navier-Stokes equations in boundary fitted coordinates;
- Multi-block decomposition of the domain into a series of structured block grids;
- Development of a dynamic LES model for a boundary fitted environment.

This methodology will be tested for simplified geometries that share significant properties with rod-bundles and then will be applied to a tight-lattice rod-bundle.

2. LES IN BOUNDARY FITTED COORDINATES

The methodology considered here solves the Navier-Stokes equations in boundary fitted coordinates (Fig. 1). This is of particular importance for LES; in fact, two spatial operations, coordinate transformation and spatial filtering, have to be performed on the Navier-Stokes equations in order to obtain the system of equations to be solved. The order of the two operations is important and translates into differences in the numerical practices that

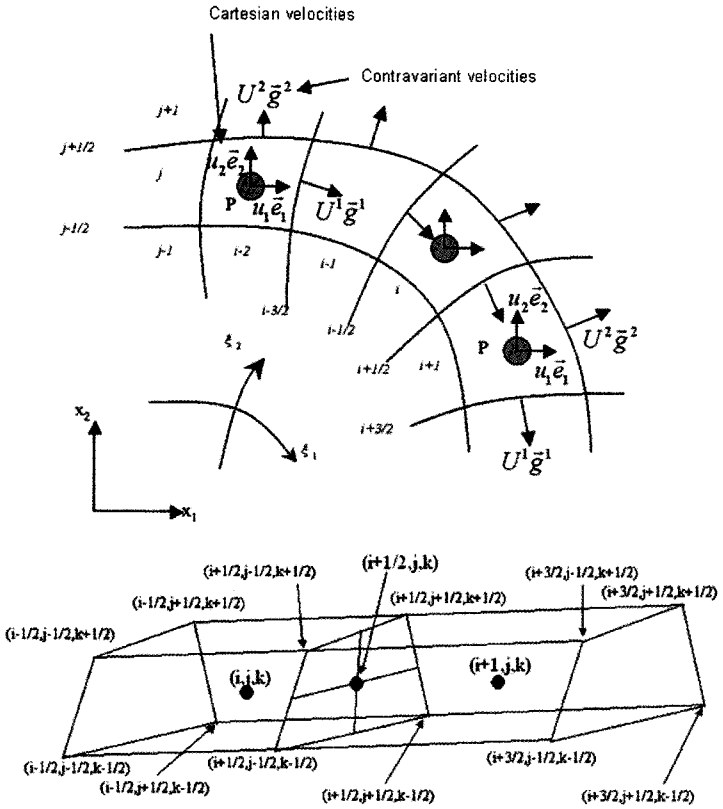

Fig. 1. Details of the Discretization

need to be employed [6]. In fact, the direct application of the filtering on the Navier-Stokes equations in a complex geometry leads to the introduction of a commutation error wherever the filter is not spatially homogeneous [7]. An alternative approach is to invert the order of the two operations. In this case the filtering takes place in the computational space where the grid is uniform by definition. The equations then become [6,8]:

$$\frac{\partial \overline{J^{-1}}\,\overline{u_i}}{\partial t}+\frac{\partial\left(\overline{U^k}\,\overline{u_i}\right)}{\partial \xi_k}=-\frac{\partial}{\partial \xi_k}\left(\left(\frac{\overline{J^{-1}\xi_i^k}\,\overline{p}}{\rho}+T_i^k\right)\right)+\nu\frac{\partial}{\partial \xi_k}\left(\overline{J^{-1}g_{kl}}\frac{\partial \overline{u_i}}{\partial \xi_l}\right) \tag{1}$$

$$\frac{\partial \overline{J^{-1}\xi_i^k}\,\overline{u_i}}{\partial \xi_k}=0 \tag{2}$$

where J is the Jacobian, g denotes the skewness tensor, and:

$$T_i^k=\overline{U^k u_i}-\overline{U^k}\,\overline{u_i}, \tag{3}$$

$$U^k=J^{-1}\xi_j^k u_j, \tag{4}$$

$$\xi_j^i=\frac{\partial \xi_i}{\partial x_j}. \tag{5}$$

The filter operator in the computational space is defined for contravariant variables, by (an example for the contravariant velocity):

$$U^k=\int_{-\infty}^{+\infty}G\left(\vec{\xi}',\vec{\xi}\right)J^{-1}\xi_j^k u_j\left(\vec{\xi}'\right)d\vec{\xi}', \tag{6}$$

where $G(\xi',\xi)$ is the filter kernel. The relationship between contravariant velocity and Cartesian velocity is given by the equation:

$$\overline{U^k}=\overline{J^{-1}\xi_j^k}\,\overline{u_j}. \tag{7}$$

The matrix $\overline{J^{-1}\xi_j^k}$ maps a filtered Cartesian quantity to its

contravariant equivalent. Its inverse G_{kj} maps a filtered contravariant quantity to its Cartesian equivalent. Jordan [8] proposed the following modification of the Smagorinsky model for boundary fitted coordinates:

$$T_i^k - \frac{1}{3}T_i^i\delta_i^k = -2C_s\Delta^2\overline{\overline{J^{-1}\xi_i^k}}\,\overline{\overline{|S|S_{ij}}}\,, \tag{8}$$

where S_{ij} is the Strain tensor and C_s is the Smagorinsky coefficient, which can be determined dynamically [9-10]. This method has been extended by Jordan [8] to boundary fitted coordinates. It can be synthesized in the following three equations if the dynamic procedure takes place in the computational space:

$$C_s = \frac{L_i^k M_i^k}{2M_i^k M_i^k}\,, \tag{9}$$

$$L_i^k = \overline{\overline{U^k u_i}} - \overline{\overline{U^k}}\,\overline{\overline{u_i}}\,, \tag{10}$$

$$M_i^k = 2\left(\overline{\overline{\Delta}}^2\overline{\overline{J^{-1}\xi_j^k}}\,\overline{\overline{|S|S_{ij}}} - \Delta^2\overline{\overline{J\xi_j^k}}\,\overline{\overline{|S|S_{ij}}}\right), \tag{11}$$

where the two bars represent a filtering with different width $\bar{\Delta}$, usually referred to as test filtering. In the present work we will use the following variant to the dynamic model [11]:

$$C_s = \frac{G_{kq}L_i^k M_i^q}{2G_{kq}M_i^k M_i^q}\,, \tag{12}$$

where G is the projection tensor discussed above. The numerator and denominator are averaged separately in the stream-wise direction.

The Sub-Grid-Scale (SGS) model (12) has been chosen after *a priori* tests [12-14] were conducted to determine which SGS model is more suitable for the simulation of flows in annular channels. In particular, the cases examined are the flow in a concentric annular channel (α=0.1, Re= 8900) and the flow in an eccentric annulus (e=0.5, α=0.5, Re=26600). Previous DNS computations [12] (Fig. 2), have been used to compute the stresses exactly through (3.1). Different models have then been compared to the DNS data. For example, Fig. 3 (left) shows a comparison between the exact instantaneous value of T_{12} (computed by using equation 3.1) and the value predicted by the dynamic mixed model [11]. It should be noticed that the agreement is excellent (Fig. 3 - left and Tab. 1). In fact the dynamic mixed model has shown itself to be the best available a priori test among the models considered. However, it has also shown instability for the problems presented here.

The dynamic model given by (12), performs well (Fig. 3 – upper right) for the direct comparison of T_{12}. Table 1 gives an extensive comparison of the performance of different models, by considering the correlation coefficient between the DNS distribution of T_{12} (given by 3.1) and the one obtained by each separate model.

In the framework of *a priori* tests, the SGS dissipation:

$$\varepsilon_{SGS} = S_{ij}\tau_{ij} \tag{13}$$

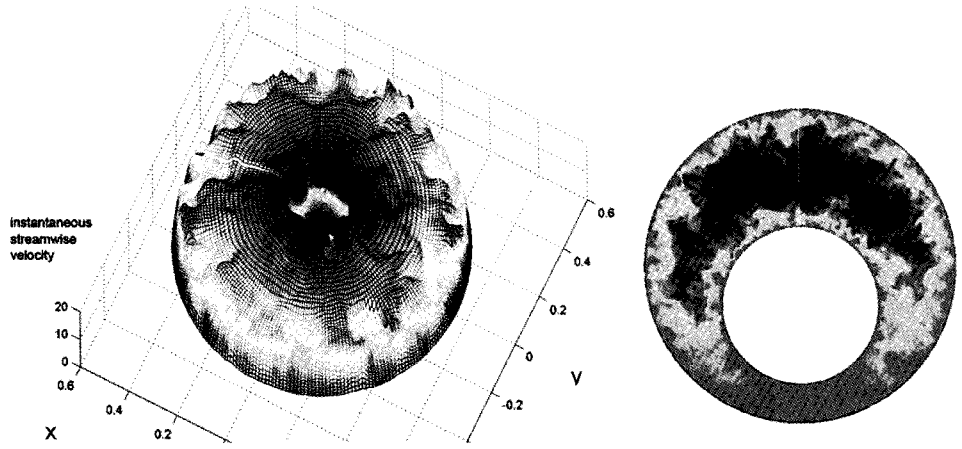

Fig. 2. Snapshot of the Streamwise Velocity of the Channel Flow in a Concentric Duct and an Eccentric Duct (Mesh 768 × 300 × 768, Re=26600, e=0.5, α=0.5), DNS Calculations Used for the *a Priori* Analysis

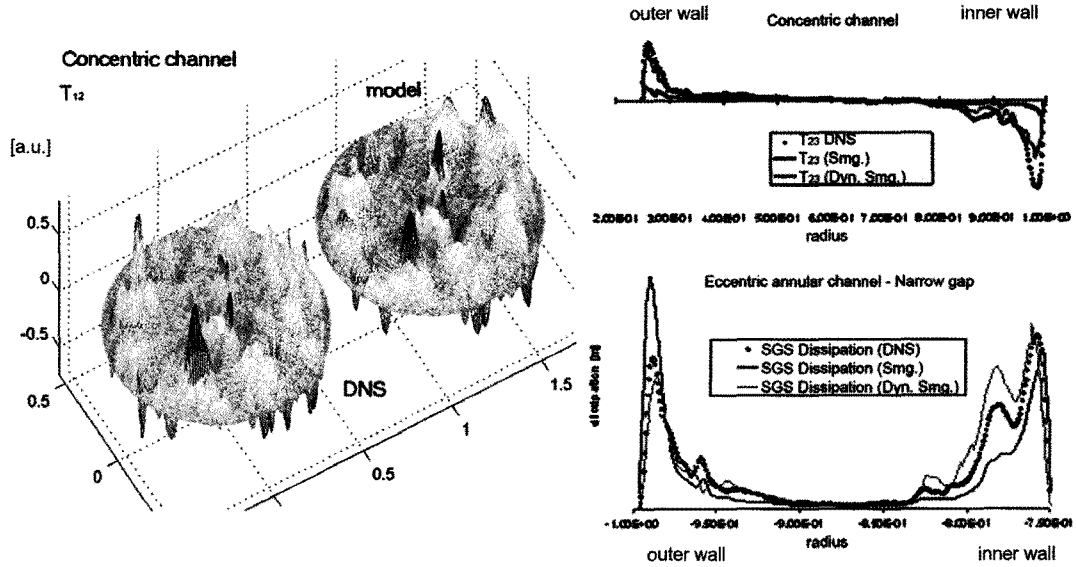

Fig. 3. A Priori Test for Concentric and Eccentric Channels. Direct Comparison for the Stresses (Left) and Comparison for the SGS Dissipation (Right)

Table 1. Correlation Coefficients for T_{12}, Comparison between Different Models at Different Reynolds Numbers

	Concentric channel (Re=8900) T_{12}	Eccentric channel (Re=13100) T_{12}	Eccentric channel (Re=26600) T_{12}
Dynamic Smagorinsky	0.18	0.15	0.15
Dynamic mixed	0.78	0.81	0.82
Smagorinsky	0.08	0.04	0.04

has been identified as the relevant quantity that should be reproduced correctly (i.e., the energy transfer from the resolved scales to the modeled scales has to be correctly modeled). Figure 3 (bottom right), shows that, for eccentric annuli, the Smagorinsky model over-predicts dissipation in the crucial near-wall region. This is also true for concentric annular channels.

3. CODE

The methodology outlined in sections 2 and 3 has been implemented in a code. The code developed is largely based upon an available pseudo-DNS code (SPARKLE-DNS [15]. Equations (2) are discretized in the following manner: the Cartesian coordinate velocities are evaluated on the cell center while the contravariant velocities are evaluated on the surface of the cells (Fig. 1). The code developed is based on the fractional step algorithm [16].

The predictor stage has been computed by the Adams-Bashforth scheme:

$$u_i^p = u_i^n + \Delta t\left(\frac{3}{2}H_i^n - \frac{1}{2}H_i^{n-1}\right) + \frac{\Delta t}{\rho}\frac{\partial \overline{P}}{\partial z}\delta_{i3}, \qquad (14)$$

where $\frac{\partial \overline{P}}{\partial z}$ is the mean velocity gradient in the streamwise direction, treated here as a body force. The terms H include convection and diffusion terms. The convection term has been discretized in the following way (considering U, the contravariant velocity in direction ξ and u is a Cartesian component):

$$U\frac{\partial u}{\partial \xi}\bigg|_{ijk} = \frac{1}{2}\left(U_{i+1/2\,jk}\frac{u_{i+1\,jk}-u_{ijk}}{\Delta\xi} + U_{i-1/2\,jk}\frac{u_{ijk}-u_{i-1\,jk}}{\Delta\xi}\right), \qquad (15)$$

where the contravariant terms are evaluated on the surfaces of the cell through a fourth order interpolation scheme. The corrector stage is given by the equation:

$$u_i^{n+1} = u_i^p - \frac{\Delta t}{\rho}\frac{\partial \xi^j}{\partial x_i}\cdot\frac{\partial p}{\partial \xi^j}\bigg|^{n+1}, \qquad (16)$$

where the gauge pressure is obtained by the solution of the Poisson equation for the pressure.
The algorithms employed for the solution of the Poisson equation are the Conjugate Gradient Squared CGS and Bi-Conjugate Gradient Stabilized [17].

Through all the simulations carried out in the present paper the CFL has been kept below 0.2. An alternative implicit predictor stage has also been developed to update the diffusion part of the operator through a Crank-Nicholson scheme when the limit due to diffusion number becomes unpractical (e.g., in eccentric channels for an high value of the eccentricity e).

For the initial condition, two strategies have been implemented:

- to use the flow field produced by a previous parallel plate simulation, mapping it upon the grid considered for the simulation;
- to superimpose the least stable perturbation [18] to the laminar solution.

4. DOMAIN DECOMPOSITION

In order to reproduce complex geometries, structured grids are limited and do not offer a sufficient level of flexibility even in a boundary fitted environment. For instance, the flow in an array of rods cannot be solved by these techniques.

A possible solution to extend the present methodology to intrinsically unstructured topologies is to decompose the domain into a series of structured blocks [19]. In the present work we will consider non-overlapping domain decomposition. The only hypothesis made in the implementation is that the grid preserves regularity on the borders of the each block. This method presents the

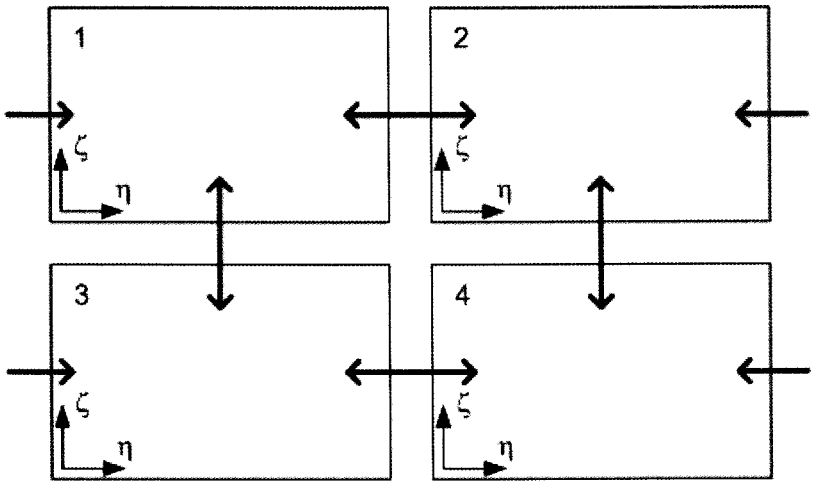

Fig. 4. Domain Decomposition

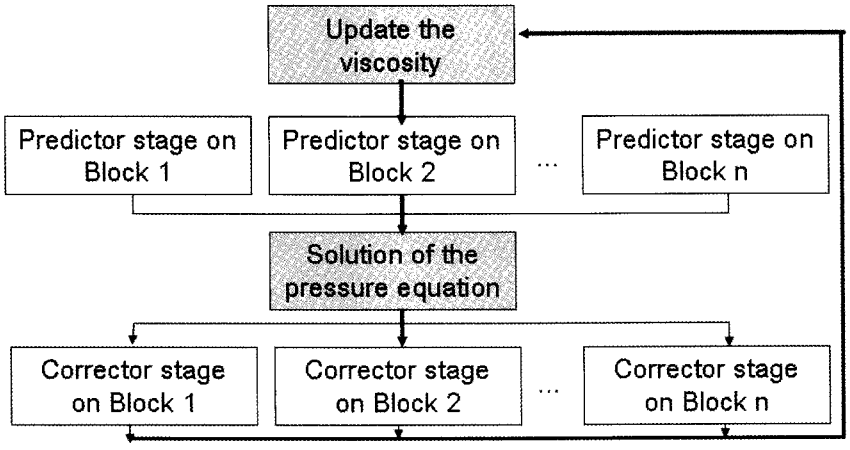

Fig. 5. Flow Structure of the Code

interesting property of being easily extended to parallel computations. An example for channel flow is shown in Fig. 4.

Predictor and corrector stages are carried out on each different block independently (Fig. 5) while the solution of the pressure Poisson equation is carried out on the domain as a whole. This ensures high accuracy for the continuity equation, which is particularly important for LES. A two-level preconditioning has been adopted [20]. Alternatively, for large scale calculations a geometric multi-grid preconditioning has also been implemented. When domain decomposition is applied only in the streamwise direction, a fast FFT solver has been used.

5. TESTING

In this section, three independent benchmarks of the code in simplified geometries will be presented. A tight-lattice rod-bundle will also be addressed. In all cases the mesh has been developed considering the following guidelines, which have proven satisfactory:

- the mesh nearest to the wall has a size smaller than one wall unit;
- in the direction normal to the wall, the maximum size of the mesh is lower than 10 wall units and at least five points are contained in the viscous sub-region ($y^+<8$);
- in the span-wise direction, the maximum size of the mesh is lower than 20 wall units;
- in the stream-wise direction, the maximum size of the mesh is lower than 30 wall units.

5.1 Parallel Plates

A parallel plate simulation has been performed at Re_τ =180, imposing the pressure gradient and periodic boundaries in the streamwise and spanwise directions. The length of the domain in the streamwise direction has been chosen coherently with the choice of the boundary condition [21] and was set to $2\pi D_h$ in the streamwise direction and πD_h in the spanwise direction.

The calculation has been performed on a global $64 \times 64 \times 64$ grid; it was decomposed in 8 sub-domains and solved with 8 processors (the domain decomposition is given in Fig. 4). A time step between 1×10^{-2} D_h/w_{bulk} and 5×10^{-3} D_h/w_{bulk} has been used. A time corresponding to 200 D_h/w_{bulk} was needed to reach convergence. A snapshot of the flow field obtained is given in Fig. 6, where it is possible to notice several streamwise rolls, typical of near wall turbulence.

Detailed results are reported for the streamwise velocity and rms of the streamwise velocity in Fig. 7. The results presented are Reynolds averaged over 100 D_h/w_{bulk}. The agreement with data obtained by DNS [22] is excellent for first order and second order statistics such as the streamwise velocity and the rms of the turbulent velocity.

Since in this case the domain decomposition has been performed in all the directions, the result gives us confidence in the effectiveness of the domain decomposition technique.

5.2 Concentric Annulus

A concentric channel with a parameter α equal to 0.1 and a hydraulic diameter equal to 0.5 has been simulated at Re=8800. The domain has been decomposed only in the streamwise direction, where periodic boundary conditions have been implemented. The length of the domain has been selected so that the two point correlation tensor between points at half-length distance will be negligible ($2\pi D_h$ was deemed sufficient). The grid employed is composed of $64 \times 128 \times 64$ (wall-normal × spanwise ×

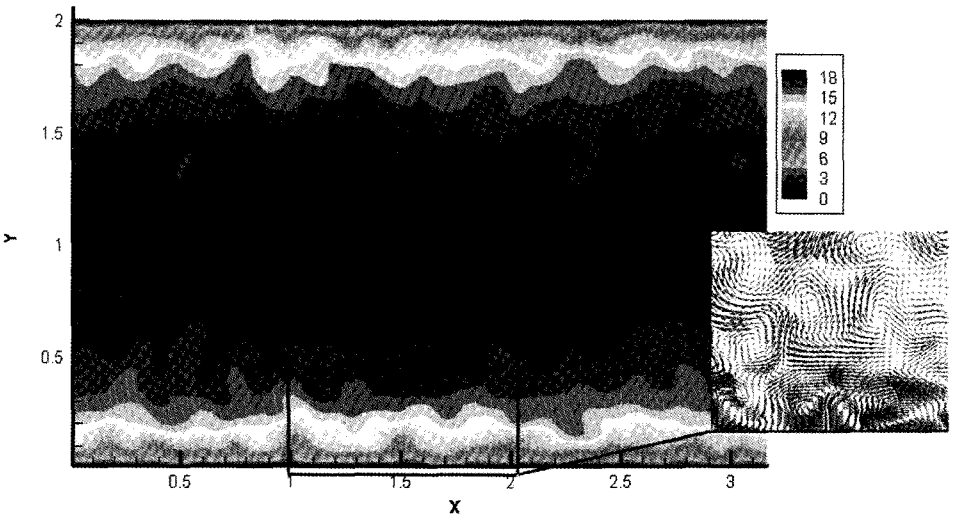

Fig. 6. Snapshot of Channel Flow, Streamwise Velocity and Velocity Vectors on the Cross Plane

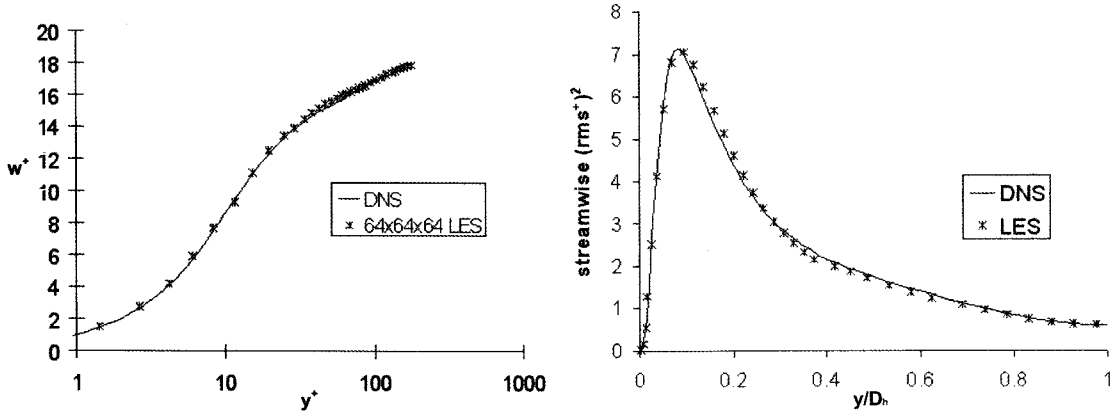

Fig. 7. Parallel Plate Flow, Streamwise Velocity and Rms of the Streamwise Velocity. Comparison with DNS Data [22] at Re=4500 (Re_τ=180)

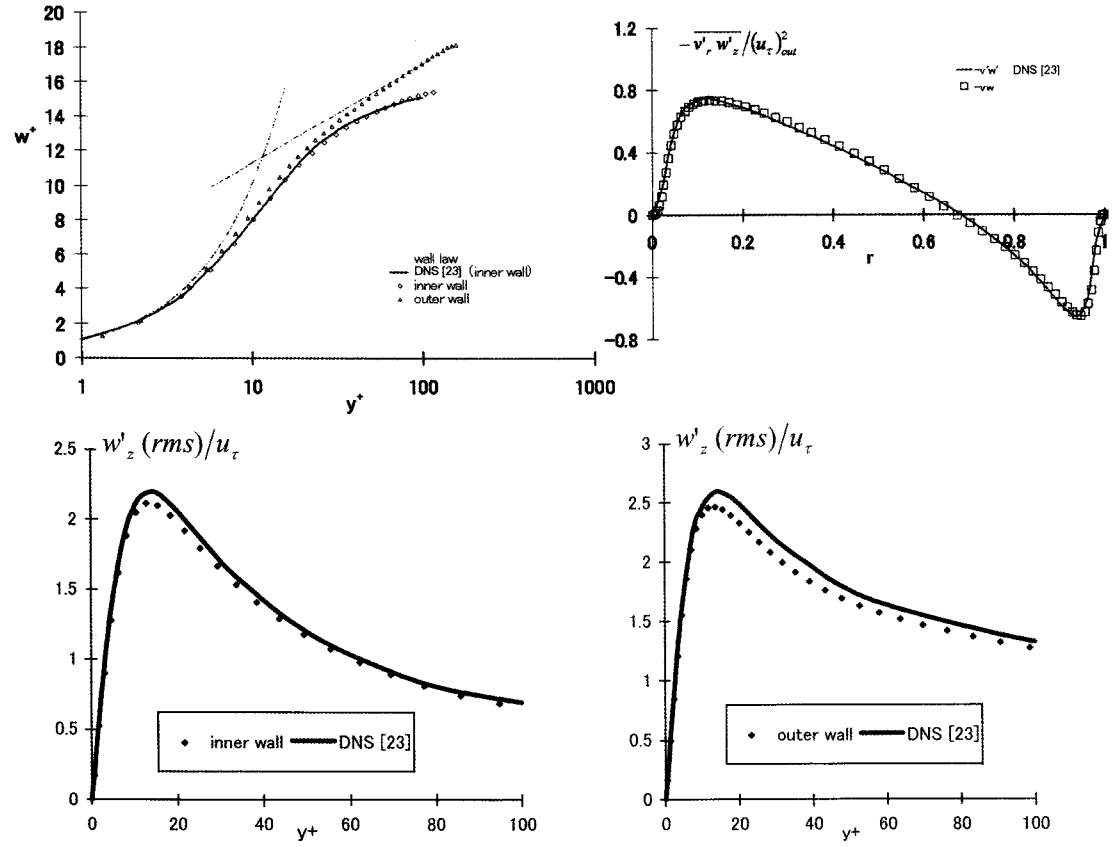

Fig. 8. Concentric Channel Average Profile

streamwise) meshes. The time step used is between 2×10^{-3} D_h/w_{bulk} and 5×10^{-3} D_h/w_{bulk}. Averaging over $300D_h/w_{bulk}$ was needed to reach convergence.

Figure 8 reports two representative graphs of the Reynolds averaged results. The agreement with DNS data appears to be excellent. The profile of the inner wall is sensibly different from the law of the wall. In fact, the presence of an internal boundary introduces features of external flows near the inner cylinder [24], such as a positive skewness of the radial velocity and lower turbulent intensities near the inner wall. Moreover, the wall shear stress on the inner wall is higher than the wall shear stress

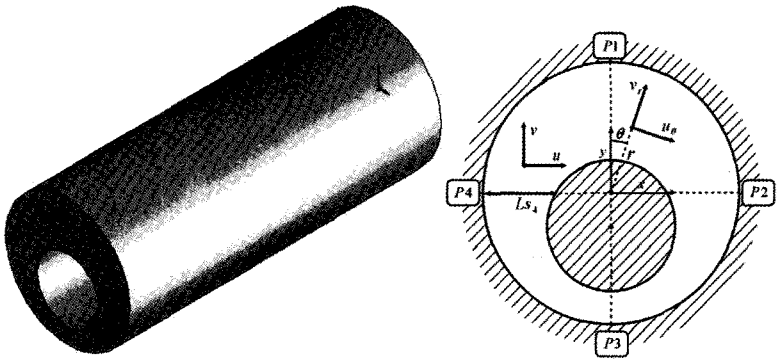

Fig. 9. Eccentric Annulus and Reference Planes

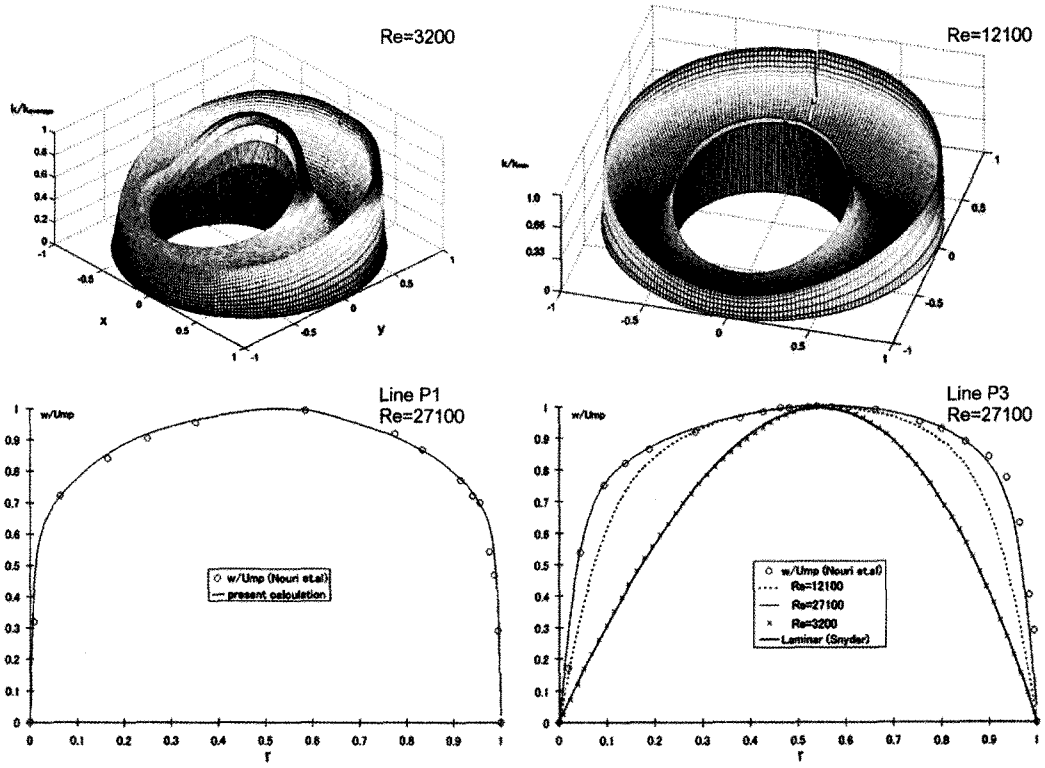

Fig. 10. Turbulent Kinetic Energy Distribution and Streamwise Velocity Distribution at Different Reynolds Numbers for α=0.5 and e=0.5, and Detail on the Lines P1 and P3

on the outer wall.

The overall redistribution of turbulent quantities and Reynolds stresses is well illustrated by the graph showing the shear stress as a function of the radial position (r represents the relative distance from the outer wall). In fact, the position of zero shear stress is off-centered (closer to inner wall) and correctly reproduced. The rms of the streamwise velocity is predicted with acceptable accuracy, especially near the inner wall (near the outer wall the mesh might be slightly too coarse).

5.3 Eccentric Annulus

Eccentric annular channel flow presents important similarities with the flow in rod-bundles and can be used as a benchmark to verify the capability of a given code to reproduce such features correctly. This work is part of a larger project [25]; the focus in the present paper will be on the effectiveness of the LES methodology. The reference geometry is reported in Fig. 9. Several values of the geometric parameters α and e and the Reynolds number have been explored.

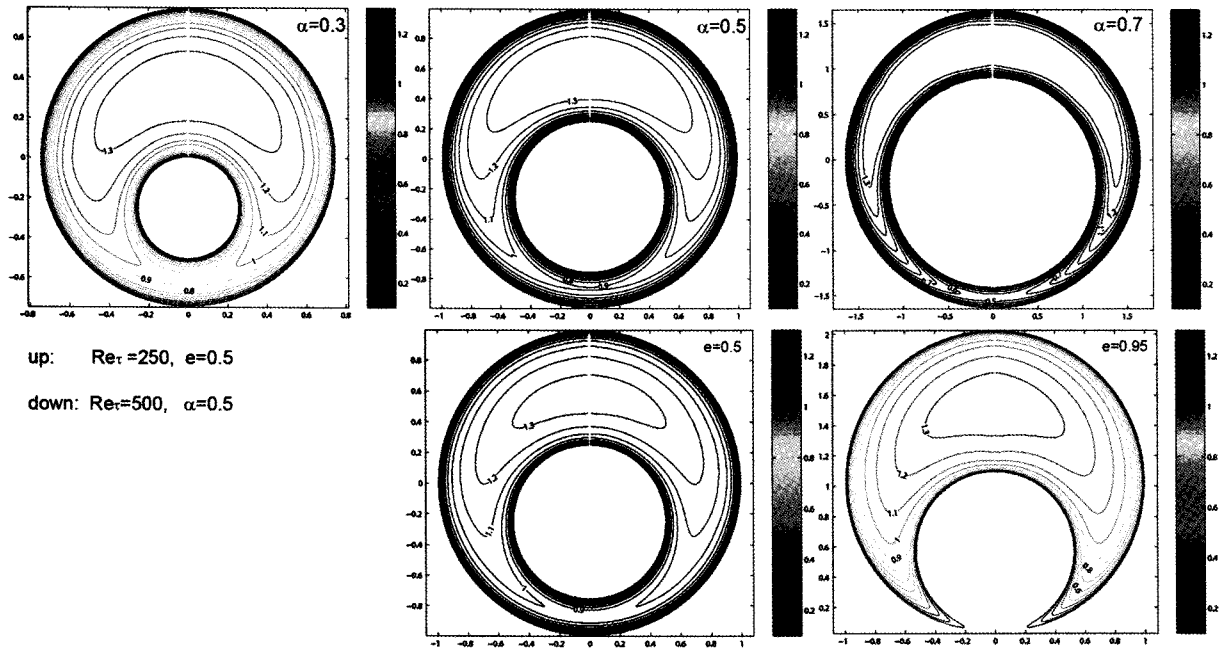

Fig. 11. Contour Plot of the Streamwise Velocity as a Ratio of the Bulk Velocity, Comparison of the Profile between Different Geometric Profiles

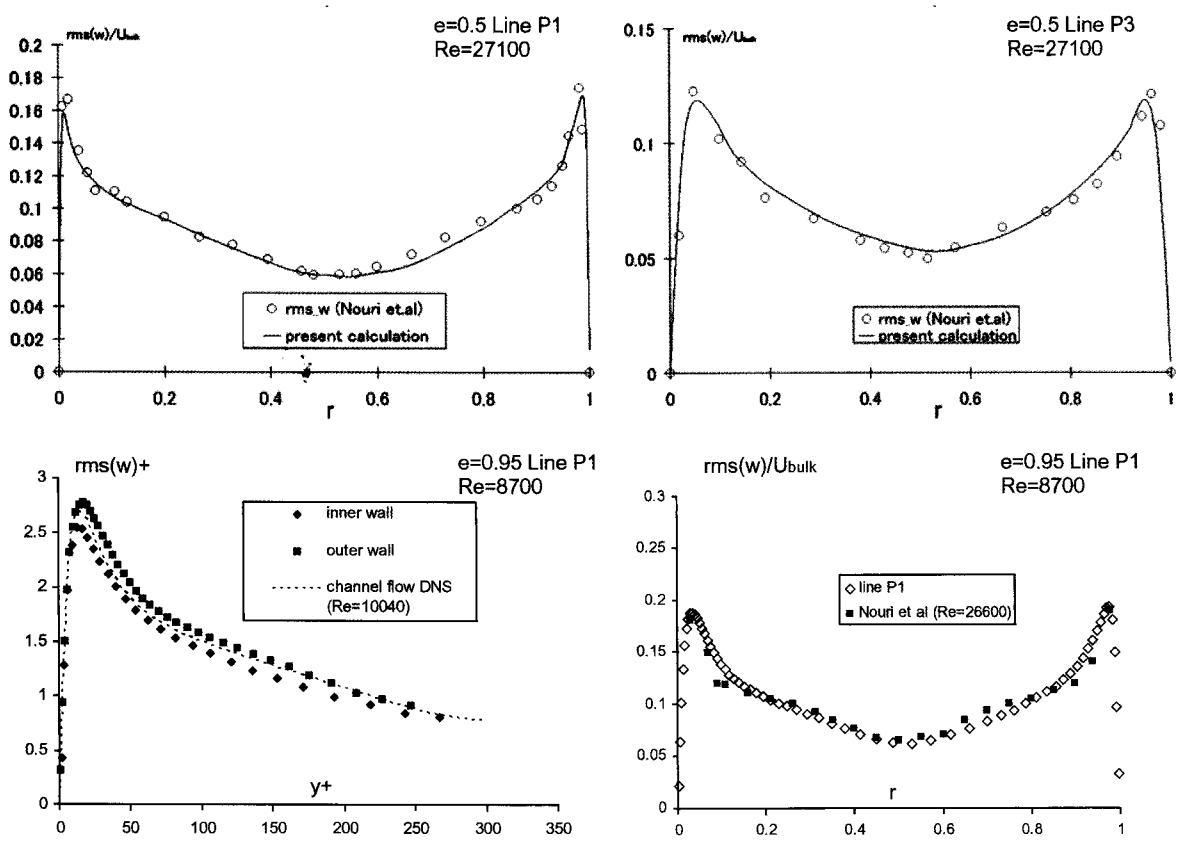

Fig. 12. Rms of the Streamwise Velocity for e=0.5 (Top) and e=0.95 (Bottom). For both Cases α=0.5

Figure 10 displays a three-dimensional graph of the turbulent kinetic energy that illustrates the Reynolds number effect on the flow field for α =0.5 and e =0.5. In particular at Re=3200, the peak of the turbulent kinetic energy in the narrow gap is not positioned near wall, clear indication that turbulence is not produced locally. At Re=12100 the peak of the turbulent kinetic energy is near wall in the whole cross section.

Figure 10 – bottom, right, compares the profile of the streamwise velocity in the narrow gap at different Reynolds numbers with experimental results [26] and a theoretical laminar solution [27] for a case with e=0.5, α=0.5. At low Reynolds numbers (Re=3200), the profile in the narrow gap is laminar while it is turbulent in the larger gap. For Re=3200 the relative maximums are equal to 1.43 and 0.92, respectively, for lines P1 and P3 (in very good agreement with the values reported by Nikitin [28]).

The case with Re=27100 has been computed with a high resolution 512 × 300 × 512 grid on Earth Simulator[1]. For this case, the local maximum of the streamwise velocity for line P1 has been found equal to 1.38 times the bulk velocity, while the same ratio was 0.855 for reference line P3 (in good agreement with the experimental results of Nouri [26]). In the wider gap the local maximum of the streamwise velocity is slightly closer to the inner cylinder (0.54 for calculation and 0.55 for the experiment – Fig. 10 bottom-right), accounting for a small effect due to transverse curvature. In general, the streamwise velocity distribution is in excellent agreement with the experiment (Fig. 10 - bottom).

Figure 11 shows the effect of the two geometric parameters on the streamwise velocity profile (the hydraulic diameter is kept constant). At constant eccentricity e=0.5, the streamwise velocity is increasingly inhomogeneous in the spanwise direction as α increases. The calculations presented in Fig. 11 have been performed on, 256 × 64 × 256, 256 × 64 × 128, and 256 × 128 × 256 grids.

Figure 12 shows the streamwise rms distribution at e=0.5, α=0.5, Re=27100 as a function of the relative distance from the outer wall for the wide gap and the narrow gap, respectively. The agreement with the experiment appears to be excellent. Other higher statistics (such as the shear stress or the rms of the other velocity components), not reported here in the interest of brevity, are in good agreement with experimental results.

Figure 12 shows also the streamwise rms for a case with e=0.95, α=0.5, Re=8700. In this case a direct comparison with the experiment was not possible (the Reynolds number of the experiment was considerably higher), but it is evident that the normalized distribution fits well with the rms of the streamwise velocity for a channel flow at a slightly higher Reynolds number (DNS [22], Re=10040) for both the inner and the outer walls.

The use of an LES allows for the study of unsteady anisotropic phenomena. It is possible to observe flow pulsations in the narrow gap area where positive and negative cross velocity areas alternate. Figure 13 shows iso-surfaces at u=2.0 m/s (16 % w_{bulk}) and u=-2.0 m/s for the case Re=3100, α=0.5, e=0.8. Coherent structures on both sides of the gap propagate in the streamwise direction, forming a vortex street that drives the pulsations. An extensive account of this phenomenon can be found in

[1] Earth Simulator was a supercomputer located in JAMSTEC (www.jamstec.go.jp) from 2001 to 2008

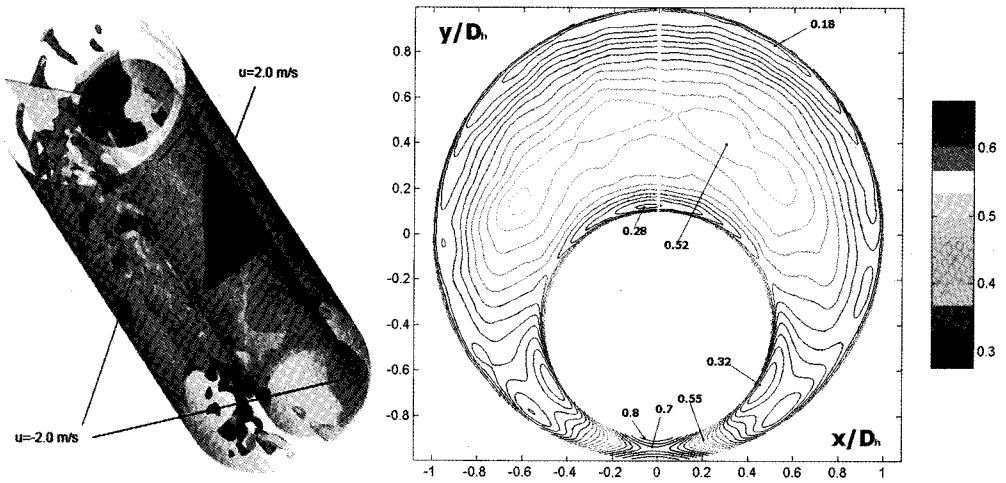

Fig. 13. Isosurfaces for Two Values of the Cross Velocity u and Energy Partition Factor f (e=0.8, α=0.5)

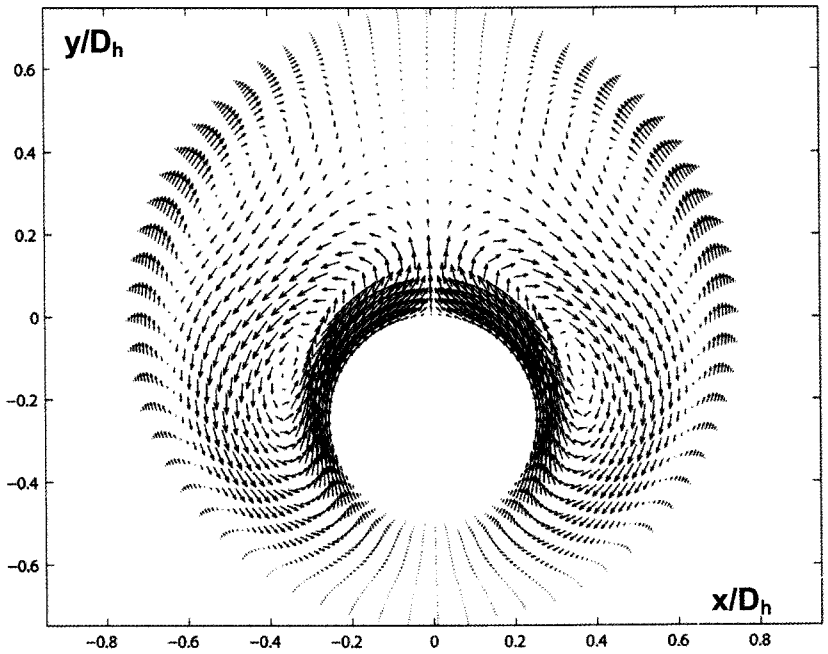

Fig. 14. Secondary Flows for a Case e=0.5, α=0.3, Re=2900

Merzari *et al.* [1] and Hopper and Rehme [2]. The pulsations are clearly present at Re<12000 for e=0.5, α=0.5. for Reynolds numbers up to 12000 for e=0.8, α=0.5. They are also present at Re=3300 for α=0.7, e=0.5 and Re=2900 for α=0.3, e=0.5. Interestingly, they have an amplitude smaller than 0.7 % of the bulk velocity for e=0.95, α=0.5, Re=8700. For this case the size of the gap might be too small and the viscous forces appear to dampen the oscillations.

When the flow field is averaged, a strong anisotropic pattern is observed in the narrow gap. Figure 13 also shows the energy partition ratio f:

$$f = \frac{\langle u'u' \rangle + \langle v'v' \rangle}{\langle u'u' \rangle + \langle v'v' \rangle + \langle w'w' \rangle} \tag{17}$$

which represents a measure of anisotropy for the same case. In the narrow gap, the streamwise velocity component of the turbulent kinetic energy is marginal, accounting for a situation in which turbulence is not produced locally through the mechanism common to bounded flows [29]. This is consistent with the results of Fig. 10. Turbulence is either transported or produced through other means. The strong anisotropy (f>0.8 in the narrow gap region) is associated with secondary flows in the cross section, whose shape depends upon the parameters e and α [25]. An example is given in Fig. 14, for a case of e=0.5, α=0.3, Re=2900. The maximum velocity is 3 % of the bulk velocity. The secondary flow pattern for this case is given by four vortices. The direction of the flow is from the wide gap to the narrow gap in the low-shear region and the opposite direction near wall.

5.4 Rod-Bundles

The methodology and the code presented in this paper can be successfully applied to the simulation of rod-bundles. The flow domain has been divided in 12 × 8 blocks (blocks in the cross section × number of slices in the streamwise direction). The calculation presented here has been run on Earth Simulator[1] for a rod-bundle with P/D=1.05 at Re=20000. The time step has been set to 1.5 10^{-3} D_h/W_{bulk} and each block was given by a 152 × 99 × 64 grid (spanwise × wall-normal × streamwise). Periodic boundary conditions have been assumed in the streamwise direction and in the cross section (Fig. 15). In the open region (at equal distance between gaps) the profile of the streamwise velocity approximates reasonably well the law of the wall (Fig. 15).

Figure 15 displays a snapshot of the velocity field in the cross section with a detail of the central gap. The vector plot shows a vortex positioned near the gap driving the cross flow between the two subchannels. The vortex extends in the streamwise direction, thus mimicking the same phenomenon described previously for eccentric channels and other related geometries [1], [2], [25]. We may conclude that, at least qualitatively, the present code is able to reproduce the fundamental phenomena involved in the turbulent mixing between sub-channels. A further assessment of this capability is provided in Merzari and Ninokata [30].

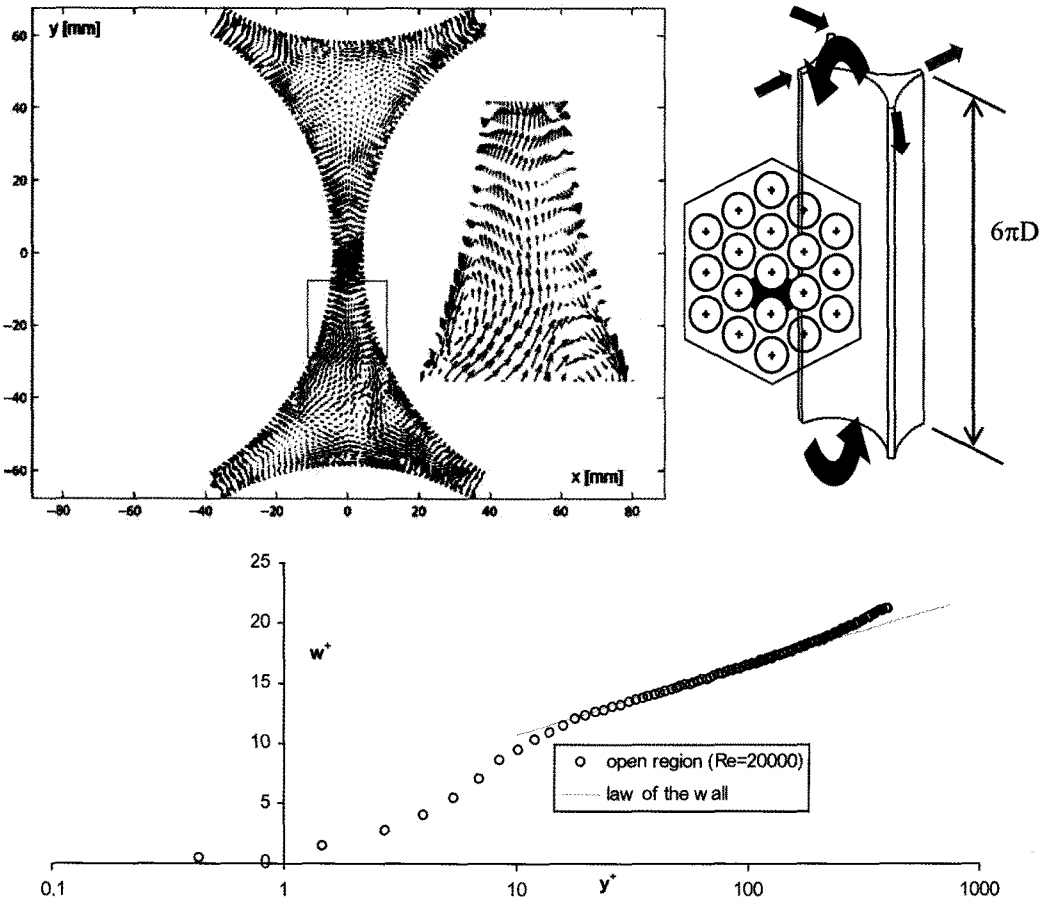

Fig. 15. Snapshot of the Velocity Field in the Cross Section. P/D=1.05, Re=20000, (Only 1/9 of the Vectors are Shown). Streamwise Velocity Profile in Wall Units Compared to the Wall of the Wall in the Open Region (Maximum Distance from the Narrow Gap)

6. CONCLUSIONS

An LES methodology has been developed for the flow in complex geometries, suitable for the simulation of fuel bundles. Its main features are: boundary fitted coordinates, multi-block domain decomposition, and a Dynamic SGS model. The code has been tested on simple flow geometry as a tool to provide accurate results and further insight into the physics of the phenomena involved. The multiblock capability has been tested on channel flow while the SGS models have been tested on geometry characterized by a configuration similar to fuel bundles (concentric and eccentric annular channels). In particular, the present code has reproduced successfully the following features for concentric and eccentric channels:

1. presence of secondary flows, and strong anisotropy in the narrow gap region (Fig. 14) [25];
2. presence of global flow pulsations (Fig. 13) [25];
3. effect of transverse curvature (Fig. 8);
4. spanwise variation of the streamwise velocity distribution and of turbulence production (Fig. 10) and occasional laminarization in the narrow gap region (Fig. 10 and 11).

Since these features are also present in rod-bundles, it is reasonable to assume that the code will also be capable of tackling rod-bundle simulations and of reproducing global flow pulsations [29]. The simulation of the flow in a tight-rod bundle presented in section 5.4 and in Merzari and Ninokata [30] seems to confirm these conclusions (Fig. 15).

Future applications of this code (and more generally of this methodology) might involve a stochastic study [5] of the flow field in rod-bundles, either with periodic boundary conditions in the direction of homogeneous turbulence or other configurations (spacers, blockage,...).

NOMENCLATURE

D_{out}	Outer diameter
D_{in}	Inner diameter
α	$=D_{in} / D_{out}$

d	Distance between the two cylinders axis, for eccentric channels
e	$= d/(D_{out} - D_{in})$
u_i, (u,v,w)	Instantaneous Cartesian velocity components
r	Relative distance from the outer wall
y	Wall distance ($=y/u_\tau$)
y^+	Normalized wall distance
x_i, (x,y,z)	Cartesian coordinates
ξ_i, (η,ξ,z)	Contravariant coordinates
ρ	Density
υ	kinematic viscosity
S_{ij}	Strain tensor
τ_{ij}	Sub-Grid Scale Reynolds tensor in the physical space
T_i^k	Sub-Grid Scale Reynolds tensor in computational space
Δ	Filter width
u_τ	Friction velocity
Re_τ	Friction Reynolds number: $Re_\tau=u_\tau D/\nu$ (the friction velocity is evaluated on the outer wall, and in the wide gap for eccentric annulus)
D_h	Hydraulic diameter
Re	Reynolds number: $Re= w_b D_h/\nu$
U_{buk},W_{buk}	Bulk velocity
U_{mp}	Maximum streamwise velocity on each plane P1, P2, P3, P4
w	Streamwise velocity
w^+	$=w/u_\tau$
$\overline{v'w'}_z$	Shear stress in concentric annuli
<uu>, <vv>, <ww>	Variance of the Cartesian velocity components

REFERENCES

[1] E. Merzari and H. Ninokata, "Unsteady Reynolds averaged Navier-Stokes simulation for an accurate prediction of the flow inside tight rod bundles", 12th NURETH, Pittsburgh - USA (2007).

[2] J.D. Hooper and K. Rehme, "Large-Scale structural effect in developed turbulent flows through closely-spaced rod arrays", *Journal of Fluid Mechanics*, **Vol. 145**, pp. 305-337 (1984)

[3] H. Ha Minh, "La Modélisation Statistique de la Turbulence: Ses Capacités et ses Limitations", *Comptes rendu de l'Academie des Sciences*, **Vol. 327**, n. 4, pp.343-358 (1999).

[4] U. Piomelli, "Large Eddy Simulation: Achievements and Challenges", *Progress in Aerospace Sciences*, **Vol. 35**, pp. 335-362 (1999)

[5] J. G. Berkooz, P. Holmes, J.L., Lumley, The proper orthogonal decomposition in the analisys of turbulent flow, *Annual Reviews of Fluid Mechanics*, **25**, pp.539-575 (1993)

[6] S.A. Jordan, "A Large Eddy simulation methodology in generalized curvilinear coordinates", *Journal of Computational Physics*, **Vol. 148**, 322-340 (1999)

[7] T.S. Lund, "On the use of discrete filters for large eddy simulation", *Annual Research Briefs*, Stanford University, 1997

[8] S.A. Jordan, "Dynamic Subgrid-Scale Modeling for Large-Eddy Simulations in Complex Topologies", *Journal of Fluids Engineering*, **Vol. 123**, 3, 619-627 (2001)

[9] M. Germano, U. Piomelli and P. Moin, "A dynamic subgrid-scale eddy viscosity model", *Phys. Fluids A.*, **Vol. 3**, 1760 (1991)

[10] C. Meneveau and J. Katz, "Scale invariance and turbulence models for large-eddy simulation", *Annu. Rev.Flu. Mech.*, **Vol. 32**, 1-32 (2000)

[11] V. Armenio and U. Piomelli, "A Lagrangian Mixed Subgrid-Scale Model in Generalized Coordinates", *Flow, Turbulence and Combustion*, **Vol. 65**, pp.51-81 (2000)

[12] E. Merzari and H. Ninokata, "Test for Large Eddy Simulation Sub-Grid Scale Models for flows in annular channels", ICAPP 2007, Nice -France (2007).

[13] C. Meneveau, "Staitistics of turbulence subgrid-scales stresses: Necessary conditions and experimental tests", *Physics of Fluids*, **Vol. 6**, 815-83, (1994)

[14] N. Park, J.Y. Yoo and H. Choi, "Toward Improved Consistency of *a priori* tests with *a posteriori* tests in large eddy simulation" , *Physics of Fluids*, **Vol. 17** (2005)

[15] T. Misawa, "Development of a numerical experimental method for the evaluation of the thermal-hydraulic design of fuel with high conversion ratio", PhD thesis-Tokyo Institute of Technology (2004)

[16] Y. Zang, R.L. Street and J.R. Koseff, "A non-staggered grid, fractional step method for time-dependent incompressible Navier-Stokes equations in curvilinear coordinates", *Journal of Computational Physics*, **Vol. 114**, 1 (1994)

[17] D.R. Fokkema, G.L. Sleijpen and H.A .Van der Vorst, "Generalized Conjugate Gradient Square", *Journal of Computational and Applied Mathematics* (1996)

[18] P.J. Schmid and D.S. Henningson, "Stability and Transition in Shear Flows", Springer (2001)

[19] T. F. Chan and T. P. Mathew, "Domain Decomposition Algorithms", *Acta Numerica*, pp. 61-143 (1994)

[20] S.H.Lee, P. Jenny and H.A. Tchelepi, "A finite-volume method with hexahedral multiblock grids for modeling flows in porus media", *Computational Geo-sciencies*, **Vol. 6**, pp. 353-379 (2002)

[21] J. Jiménez and P. Moin, "The minimal flow unit in near-wall turbulence", *Journal of Fluid Mechanics*, **Vol. 225**, pp. 213-240 (1991)

[22] N. Kasagi, K. Horiuti, Y. Miyake, T. Miyauchi and Y. Nagano, "Establishment of the Direct Numerical Simulation Data Bases of Turbulent Transport Phenomena"- http://www.thtlab.t.u-tokyo.ac.jp/

[23] S. Y. Chung, G. H. Rhee and H. J. Sung, "Direct numerical simulation of turbulent concentric annular pipe flow, Part 1: Flow field", *International Journal of Heat and Fluid Flow*, **Vol. 23**, pp. 426-440 (2002)

[24] J.C. Neves, P. Moin and R.D. Moser, "Effects of convex transverse curvature on wall-bounded turbulence. Part 1. The velocity and vorticity", *J. Fluid Mechanics*, **Vol. 272**, pp. 349-382 (1973)

[25] E. Merzari and H.Ninokata, "Anisotropy and Coherent Structures for the flow in Annular Channels", *Flow, Turbulence and Combustion*, **Vol. 82**, pp. 93-120 (2009)

[26] J.M. Nouri, H. Umur and J.H. Whitelaw, "Flow of Newtonian and non-Newtonian fluids in concentric and eccentric annuli", *Journal of Fluid Mechanics*, **Vol. 253**, pp. 617-64, (1993)

[27] W.T. Snyder and G.A. Goldstein, "An analysis of Fully

Developed Laminar Flow in an Eccentric Annulus", *A.I.Ch.E. Journal*, **Vol. 11**, 462-467 (1965)

[28] N.V. Nikitin, "Direct Numerical Simulation of turbulent flows in eccentric pipes", *Computational Mathematics and Mathematical Physics*, **Vol.46**, 509-526 (2006)

[29] S. B. Pope, Turbulent Flows, Cambridge University Press, 2000

[30] E. Merzari and H.Ninokata, "Proper Orthogonal Decomposition of the Flow in a Rod-Bundle", Proceedings of NURETH-13, Sept. 27th-Oct. 2nd 2009, Kanazawa, Japan